Supplemental Material

SUPPLEMENTARY INFORMATION to:

"Compatible Fossil Fuel CO_2 emissions in the CMIP6 Earth System Models' Historical and Shared Socioeconomic Pathway experiments of the 21st Century"

by

Spencer K. Liddicoat, Andy J. Wiltshire, Chris D. Jones, Vivek K. Arora, Victor Brovkin, Patricia Cadule, Tomohiro Hajima, David M. Lawrence, Julia Pongratz, Jörg Schwinger, Roland Séférian, Jerry F. Tjiputra, Tilo Ziehn

CONTENTS

Descriptions of Earth System Models

a. ACCESS-ESM1.5

ACCESS-ESM1.5 ((Ziehn et al. 2020) is comprised of several component models. The atmospheric model is the UK Met Office Unified Model at version 7.3 (Martin et al., 2010; The HadGEM2 Development Team, 2011) with their land surface model replaced with the Community Atmosphere Biosphere Land Exchange (CABLE) model (Kowalczyk et al., 2013) using a horizontal resolution of 1.875 ◦ x 1.25 ◦ and 38 vertical levels.

The ocean component is the NOAA/GFDL Modular Ocean Model (MOM) at version 5 (Griffies, 2014) with the same configuration as the ocean model component of ACCESS1.0 and ACCESS1.3 (Bi et al., 2013) using a 1° resolution (but finer between 10S-10N and in the Southern Ocean) and 50 vertical levels. Sea ice is simulated using the LANL CICE4.1 model (Hunke and Lipscomb, 2010). Coupling of the ocean and sea-ice to the atmosphere is through the OASIS-MCT coupler (Valcke, 2013) with a coupling frequency of 3 hours. The physical climate model configuration used here is very similar to the version (ACCESS1.3) that contributed to the Coupled Model Intercomparison Project Phase 5 (CMIP5) (Bi et al., 2013).

The carbon cycle is included in ACCESS through the CABLE land surface model and its biogeochemistry module, CASA-CNP (Wang et al., 2010), and through the World Ocean Model of Biogeochemistry and Trophic-dynamics (WOMBAT) (Oke et al., 2013). The WOMBAT model is based on a NPZD (nutrient-phosphate, phytoplankton, zooplankton and detritus) model with the additions of bio-available iron limitation, dissolved inorganic carbon, calcium carbonate, alkalinity and oxygen. Productivity drives uptake and formation of carbon and oxygen which exchange with the atmosphere. Sinking and remineralization of detritus carries biogeochemical tracers to the deep ocean. Iron is supplied by dust deposition, continental shelves and background ocean values. The Australian community model CABLE simulates the fluxes of momentum, heat, water and carbon at the surface. The biogeochemistry module CASA-CNP simulates the flow of carbon and nutrients such as nitrogen and phosphorus between three plant biomass pools (leaf, wood, root), three litter pools (metabolic, structural, coarse woody debris) and three organic soil pools (microbial, slow, passive) plus one inorganic soil mineral nitrogen pool and three phosphorus soil pools. In the CABLE configuration applied here we use 10 vegetated types and 3 non-vegetated types. CABLE calculates gross primary production (GPP) and leaf respiration at every time step using a two-leaf canopy scheme (Wang and Leuning, 1998) as a function of the leaf area index (LAI). Our set-up uses a simulated (prognostic) LAI based on the size of the leaf carbon pool and the specific leaf area. Daily mean GPP and leaf respiration values are then passed onto CASA CNP to calculate daily respiration fluxes and the flow of carbon and nutrients between the pools. Similar to the previous version, ACCESS-ESM1 (Law et al., 2017, Ziehn et al., 2017), we are running with nitrogen and phosphorus limitation

enabled. The land use scheme in ACCESS-ESM1.5 accounts for an annual net change in the tile fractions in each grid cell. It does not attempt to account for primary and secondary vegetation. Harvested wood is equally allocated to 3 wood harvest pools with different turnover rates. Crop harvest and grazing are not considered. Nitrogen and phosphorus pools are treated in a similar manner to the equivalent carbon pools.

b. CanESM5

CanESM5 is the fifth generation Earth System Model of the Canadian Centre for Climate Modelling and Analysis (CCCma). It has evolved from its predecessor CanESM2 (Arora et al. (2011)) that was used in CMIP5. CanESM5 represents a major update to CanESM2 and described in detail in Swart et al. (2019). The major changes relative to CanESM2 are the implementation of completely new models for the ocean, sea-ice, marine ecosystems, and a new coupler. The resolution of CanESM5 (T63 or 2.8° in the atmosphere and 1° in the ocean) remains similar to CanESM2, and is at the lower end of the spectrum of CMIP6 models. The atmospheric component of CanESM5, represented by version 5 of the Canadian Atmospheric Model (CanAM5), has several improvements relative to its predecessor, CanAM4 (von Salzen et al. (2013)).

The land surface in CanESM5 is modelled using the Canadian Land Surface Scheme (CLASS; Verseghy (2000)) and the Canadian Terrestrial Ecosystem Model (CTEM; Arora and Boer (2005); Arora and Boer (2010)) which together form the land component of CanESM5. CLASS-CTEM simulate the physical and biogeochemical land surface processes, respectively, and together they calculate fluxes of energy, water, CO_2 and wetland CH4 emissions at the land-atmosphere boundary. The introduction of dynamic wetlands and their methane emissions is a new biogeochemical process added since the CanESM2 (Arora et al. (2018)). Nitrogen cycle over land is not represented but the effect of photosynthesis down-regulation as CO_2 increases is represented.

The magnitude of the parameter representing this down-regulation is increased in CanESM5, compared to CanESM2, following Arora and Scinocca (2016) who found best value of this parameter that reproduced various aspects of the historical carbon budget for CanESM4.2 (a model version more similar to CanESM2 than CanESM5). Other than wetlands, and the changes to the strength of the CO_2 fertilization effect, the remaining terrestrial ecosystem processes are represented the same as in CanESM2. The physical ocean component of CanESM5 is based on NEMO version 3.4.1. Sea ice is represented using the LIM2 sea ice model (Bouillon et al. (2009); Fichefet and Maqueda (1997)). Ocean carbon cycle is represented using the Canadian Model of Ocean Carbon (CMOC) which was developed for earlier versions of CanESM (Arora et al. (2011); Christian et al. (2010)), and includes carbon chemistry and biology. The biological component is a simple Nutrient-Phytoplankton-Zooplankton-Detritus (NPZD) model, with fixed Redfield stoichiometry, and simple parameterizations of iron limitation, nitrogen fixation, and export flux of calcium carbonate.

c. CESM2

The Community Earth System Model version 2 (CESM2, Danabasoglu et al., 2020) couples the Community Atmosphere Model (CAM6, Simpson et al., 2020), the Community Land Model (CLM5, Lawrence et al., 2019), the Parallel Ocean Program model (POP2), and the Community Ice Sheet Model (CICE5). Full model descriptions and the performance of each component are described in the above references and references therein and in additional manuscripts in the AGU Special Issue on CESM2.

Land biogeochemistry in CESM2 is represented by CLM5, which is the latest version of CLM and includes many updates to biogeophysical and biogeochemical and land use processes relative to prior CLM versions. These updates include: revised parameterizations and structure for hydrology and snow (spatially explicit soil depth, dry surface layer, revised groundwater scheme, revised canopy interception and canopy snow processes, updated fresh snow density, simple firn model, and Model for Scale Adaptive River Transport); plant hydraulics and hydraulic redistribution; revised nitrogen cycling (flexible leaf stoichiometry, leaf N optimization for photosynthesis, carbon costs for plant nitrogen uptake); global crop model with six crop types and time-evolving irrigated areas and fertilization rates; updated stomatal physiology; updated fire model that includes deforestation/degradation fires; and new parameter estimates for many key carbon cycle and other parameters. In CLM5, vegetation distributions are prescribed according to MODIS and the land use transitions from the Land Use Harmonization dataset (LUH2, Hurtt et al. (2020)) CLM5 represents 14 natural plant functional types (PFTs) and 6 crop functional types. The vegetation state (LAI, phenology, canopy height) is prognostic in the biogeochemistry configuration used in default CESM2. This configuration includes full carbon and nitrogen cycling. PFTs on the naturally-vegetated land unit compete for water and nutrients. Deforestation in the model is represented by contraction of tree PFT area within the natural vegetated land unit, as specified by a forcing dataset. CLM5 appears to better capture CO2 and N-fertilization effects compared to observations (Wieder et al., 2019), though there are strong parameteric sensitivities in these responses (Fisher et al., 2019).

Ocean biogeochemistry in CESM2 is represented by the Marine Biogeochemistry Library (MARBL), which is configured to implement an updated version of what has previously been known as the Biogeochemistry Elemental Cycle (BEC; Moore et al., 2013). MARBL represents multiple nutrient colimitation (N, P, Si, and Fe) with three explicit phytoplankton functional groups (diatoms, diazotrophs, and pico/nano phytoplankton) and one implicit group (calcifiers). There is also one zooplankton group. MARBL prognoses carbonate chemistry and simulates sinking particulate organic matter implicitly, subject to ballasting by mineral dust, biogenic CaCO3, and Si. Updates relative to CESM1 include a representation of subgrid-scale variations in light, variable C:P stoichiometry, burial of material at the seafloor that matches riverine inputs in the preindustrial climate, both semilabile and refractory dissolved organic material pools, prognostic oceanic emission of ammonia, and an explicit ligand tracer that complexes iron.

Atmospheric deposition of iron is computed as a function of dust and black carbon deposition simulated by CAM6. Riverine nutrient, carbon, and alkalinity fluxes are supplied to the ocean from a data set.

d. CNRM-EMS2-1

Centre National de Recherches Met´ eorologiques (CNRM) CNRM-ESM2-1 CNRM-ESM2-1 is the second generation Earth System model developed by CNRM-CERFACS for CMIP6 (Séférian et al. (2019)). The atmosphere component of CNRM-ESM2-1 is based on version 6.3 of the global spectral model ARPEGE-Climat (ARPEGE-Climat v6.3). Over the land surface, CNRM-ESM2-1 use the ISBA-CTRIP land surface modeling system to solve energy, carbon and water budgets at the land surface (Decharme et al. (2019); Delire et al. (2019)).

To simulate the land carbon cycle and vegetation-climate interactions, ISBA-CTRIP simulates plant physiology, carbon allocation and turnover, and carbon cycling through litter and soil. It includes a module for wild fires, land use and land cover changes, and carbon leaching through the soil and transport of dissolved organic carbon to the ocean. Leaf photosynthesis is represented by the semi-empirical model proposed by Goudriaan et al. (1985). Canopy level assimilation is calculated using a 10-layer radiative transfer scheme including direct and diffuse radiation. Vegetation in ISBA is represented by 4 carbon pools for grasses and crops (leaves, stem, roots and a non-structural carbohydrate storage pool) with 2 additional pools for trees (aboveground wood and coarse roots). Leaf phenology results directly from the carbon balance of the leaves. The model distinguishes 16 vegetation types (10 tree and shrub types, 3 grass types and 3 crop types) alongside desert, rocks and permanent snow. In the absence of nitrogen cycling within the vegetation, an implicit nitrogen limitation scheme that reduces specific leaf area with increasing CO_2 concentration was implemented in ISBA following the meta-analysis of Yin (2002). Additionally, there is an ad-hoc representation of photosynthesis down-regulation. The litter and soil organic matter module is based on the soil carbon part of the CENTURY model (Parton et al. (1988)). The 4 litter and 3 soil carbon pools are defined based on their location above- or below-ground and potential decomposition rates. The litter pools are supplied by the flux of dead biomass from each biomass reservoir (turnover). Decomposition of litter and soil carbon releases CO_2 (heterotrophic respiration). During the decomposition process, some carbon is dissolved by water slowly percolating through the soil column. This dissolved organic carbon is transported by the rivers to the ocean.

The ocean component of CNRM-ESM2-1 is the NEMO vn3.6 (Madec et al. (2017)) which is coupled to both the GELATO sea-ice model (Salas-Melia (2002)) version 6 and also the marine biogeochemical model PISCESv2-gas.

The atmospheric chemistry scheme of CNRM-ESM2-1 is REPROBUS-C v2. This scheme resolves the spatial distribution of 63 chemistry species but does not represent the low troposphere ozone non-methane hydrocarbon chemistry. CNRM-ESM2-1 also includes an interactive tropospheric aerosol scheme included in the atmospheric component ARPEGE-Climat. This aerosol scheme, TACTIC v2, represents the main anthropogenic and natural aerosol species of the troposphere.

The ocean biogeochemical component PISCESv2 (Aumont et al. (2015). PISCESv2-gas simulates the distribution of five nutrients (from macronutrients: nitrate, ammonium, phosphate, andsilicate to micronutrient: iron) which regulate the growth of two explicit phytoplankton classes (nanophytoplankton and diatoms). Dissolved inorganic carbon (DIC) and alkalinity (Alk) are involved in the computation of the carbonate chemistry.

At ocean surface, PISCESv2-gas exchanges carbon, oxygen, dimethylsulfide (DMS) and nitrous oxide (N2O) tracers with the atmosphere using the revised air-sea exchange bulk as published by Wanninkhof (2014). PISCESv2-gas uses several boundary conditions which represent the supply of nutrients from five different sources: atmospheric deposition, rivers, sediment mobilization, sea-ice and hydrothermal vents.

e. IPSL-CM6A-LR

IPSL-CM6A-LR, is an ocean-atmosphere-land coupled model. It merges three different models that respectively simulate the atmospheric general circulation (LMDZ, v6A-LR, Peylin et al. (2020)), the oceanic general circulation (NEMO v3.6, Aumont et al. (2015); Madec et al. (2017); Rousset et al. (2015); Vancoppenolle et al. (2009)), and the land surface processes (ORCHIDEE, v2.0, Peylin et al. (2020), in preparation). The resolution of the model is 2.5° x 1.3°, with 79 vertical layers. NEMO v6A-LR is based on three sub-models for the simulation of the ocean physics (model OPA, Madec et al. (2017)), of the sea-ice physics (LIM-3, Rousset et al. (2015); Vancoppenolle et al. (2009)) and of the ocean biogeochemistry (PISCES, Aumont et al. (2015)).

The general horizontal resolution of the model is 1° in the zonal and meridional directions. It decreases to $1/3^\circ$ in the Tropics. PISCES simulates different sizes of phytoplankton and the biogeochemical cycles of carbon, iron, nitrate, silicate and phosphorus. ORCHIDEE v2.0 models the fluxes between the terrestrial surface and the atmosphere and calculates carbon, water and energy budgets (Krinner et al. (2005); Peylin et al. (2020), in preparation). The model needs light availability, CO_2 concentration, soil moisture and temperature for the simulation of the photosynthesis (Farquhar et al. (1980) and Collatz et al. (1992)). This version provides new features such as a downregulation which enables, even in the absence of an explicit nitrogen cycle representation, to account for the impact of nitrogen limitation on the CO_2 fertilization effect. This latter feature is based on a logarithmic function of the CO_2 concentration relative to 380 ppm. This leads to a decrease of the maximum rate of the photosynthesis when there is an increase of atmospheric CO_2 concentration as described by Sellers et al. (1996). The carbon assimilated by plants is distributed in 8 biomass compartments with different turnover. There are 4 litter pools. A fraction of the decomposed litter is distributed in 3 organic carbon pools. This version of ORCHIDEE is based on different time resolutions which depend on the components of the model. For instance, it is quarterly-hour for the photosynthesis and the water budgets and it is daily for the variation of the carbon storage. The spatial resolution of the vegetation depends on the type of vegetation (Plant functional types, PFTs) (Cramer (1997); Prentice et al. (1992); Wullschleger et al. (2014)). A total number of 15 PFTs are used that are divided into three groups: Forests (8), grasses and crops (6) and bare soil (1). Specific soil types are associated to these three groups. This leads to a partitioning of the grid box into three tiles.

f. MIROC-ES2L

Team MIROC (Japan Agency for Marine-Earth Science and Technology, the University of Tokyo, the National Institute for Environmental Studies) MIROC-ES2L (Hajima et al., 2020) is based on the global climate model MIROC5.2 (Tatebe et al., 2018), which is a minor updated version of MIROC5 used for CMIP5 (Watanabe et al., 2010). The physical core shares almost the same structure and characteristics with the latest model MIROC6 (Tatebe et al., 2019), except for the atmospheric spatial resolution and treatment of cumulus clouds. This model interactively couples an atmospheric general circulation model (CCSR-NIES AGCM, Tatebe et al., 2019); an on-line aerosol component (SPRINTARS, Takemura et al., 2000), an ocean GCM with a sea ice component (COCO, Hasumi, 2015); a land physical surface model (MATSIRO, Takata et al., 2003); a land biogeochemical model (VISIT, Ito and Inatomi, 2012); and an ocean biogeochemical component (OECO2, Hajima et al., 2020).

The atmospheric grid resolution is approximately 2.81◦ with 40 vertical levels between the sur-face and about 3 hPa. For the ocean, the model employs a tripolar coordinate system with 62 vertical levels. To the south of 63◦ N, the ocean model has longitudinal grid spacing of about 1◦, while the meridional grid spacing varies from about 0.5◦ near the Equator to 1◦ in the midlatitudes. Over the Arctic ocean the grid resolution is even finer following the tripolar coordinate system. The physical terrestrial component resolves the vertical soil profile with six layers down to a 14 m depth, with two types of land use tiles (agriculture and non-agriculture). Terrestrial biogeochemical component considers two layers of soil organic matter (the upper litter layer and the lower humus layer), with five types of land use tiles (primary vegetation, secondary vegetation, urban, crop, and pasture).

The terrestrial biogeochemical component simulates the global carbon cycle with fixed vegetation distribution, based on the C pools of vegetation (leaf, stem, and root), litter (leaf, stem, and root), and humus (active, intermediate, and passive). The carbon cycle processes are coupled with nitrogen cycle, and the photosynthetic capacity is controlled by leaf N concentration. The N cycle is simulated with N pools of vegetation (canopy and structural), organic soil (litter, humus, and microbe), and inorganic nitrogen (ammonium and nitrate). The model simulates the perturbation of land use change on the biogeochemistry based on the five types of land tiles in each land grid. Crop harvesting, nitrogen fixation by N-fixing crops, grazing pressure on pasture and rangeland, and the decay of organic matter in product pools are considered, all of which perturb the land biogeochemistry even when land-use is fixed at preindustrial condition. In addition, the historical and SSPs simulations considers the forest harvesting and recovery following the LUC transitions, assuming gross transitions among the land-use types. Deforestation brings the carbon and nitrogen in the harvested biomass to three types of product pools. Further details on carbon cycle processes in the model can been found in Ito and Oikawa (2002), nitrogen cycle and land-use change in Hajima et al. (2020). The new

ocean biogeochemical component model, OECO2, is a NPZD-type model and modified from the previous model (Watanabe et al., 2011). The biogeochemical compartments of OECO2 are nitrate, phosphate, dissolved iron, dissolved oxygen, two types of phytoplankton (non-diazotroph and diazotroph), zooplankton, and particulate detritus. There exist other compartments of dissolved inorganic carbon (DIC), total alkalinity, calcium, calcium carbonate, and N2O. All organic materials have an identical elemental stoichiometric ratio. The model considers external nutrient inputs (atmospheric N and Fe deposition, inorganic N and P from rivers, biological N fixation, Fe input from ocean bottom and shelf) and nutrient loss (denitrification for N and loss into sediment for N, P, and Fe). The emission, transportation, and deposition processes of iron are explicitly simulated by the atmospheric aerosol component.

g. MPI-ESM1.2-LR

The Max-Planck Institute for Earth System Model (MPI-ESM-1.2.0) couples the submodels of MPIOM1.6 for ocean physics, HAMOCC6 for ocean biogeochemistry, ECHAM6.3 for the atmosphere and JSBACH3.2 for the land surface (Mauritsen et al. 2019). Key improvements over the CMIP5 version include refinement of the representation of land processes by introducing amulti-layer soil hydrology scheme(Hagemann and Stacke 2015), extending the land biogeochemistry to include the nitrogen cycle (Goll et al. 2017), replacing the soil and litter decomposition by YASSO (Goll et al. 2015) and improving the representation of wildfires including the SPITFIRE model (Lasslop et al. 2014). The MPI-ESM includes both dynamic biogeographic changes in vegetation distribution and land-use induced changes. The land use change module captures subgrid scale (gross) transitions between pasture, cropland and several natural vegetation types and includes wood harvesting (Reick et al. 2013). The ocean biogeochemistry was improved by representing cyanobacteria prognostically in order to capture the response of nitrogen fixation to changing climate conditions, and further includes improved detritus settling and numerous other refinements (Paulsen et al. 2017).

h. NorESM2-LM

NorESM2 is based on the Community Earth System Model, release 2.1 (CESM2.1, Danabasoglu et al. 2020). It keeps the original land and sea-ice components of CESM2.1 (i.e., CLM5 and CICE5), while the atmospheric component is CAM6 (as in CESM), but with modifications regarding the energy and angular momentum conservation (Toniazzo et al. 2020). Further, the aerosol module of CAM6 has been replaced by the production-tagged aerosol scheme described by Kirkevag et al. (2018). The ocean physical and biogeochemical components of NorESM2 are the isopycnal ocean circulation model BLOM (Bergen Layered Ocean Model) with its carbon cycle module iHAMOCC (Tjiputra et al. 2020).

For CMIP6, NorESM2 has been run in two different resolutions: NorESM2-LM denotes a configuration with low resolution atmosphere/land models (about 2 degrees) and medium resolution ocean/ice models (nominally 1 degree resolution). The NorESM2 model is described in detail by Seland et al. (2020). The CLM5 (Community Land Model version 5, Lawrence et al. (2019)) prognostically simulates the carbon and nitrogen cycles, which include natural vegetation, crops, and soil biogeochemistry. The carbon and nitrogen budgets comprise leaf, live stem, dead stem, live coarse root, dead coarse root, fine-root, and grain pools. Each of these pools has short-term and long-term storage of non-structural carbohydrates and labile nitrogen. In addition to the vegetation pools, CLM includes a series of decomposing carbon and nitrogen pools as vegetation successively breaks down to coarse woody debris, and/or litter, and subsequently to soil organic matter.

The ocean carbon cycle component iHAMOCC in NorESM2 originated from the HAMburg Ocean Carbon Cycle Model (HAMOCC; Maier-Reimer and Wetzel, Ilyina et al. (2013)), which has been adopted to the isopycnic ocean general circulation model. The current iHAMOCC version includes new processes, refined parametrizations, as well as new diagnostic tracers (see Tjiputra et al. (2020) for details). The ecosystem model is an NPZD-type model with multi nutrient limitation in its phytoplankton growth formulation. Riverine fluxes of inorganic and organic carbon as well as nutrients are now implemented. A new feature of NorESM2 is the coupling of the atmospheric aerosol chemistry with ocean biogeochemistry through sea-to-air dimethyl sulfate (DMS) fluxes. These fluxes can alter the atmospheric radiative forcing through changes in aerosol and cloud properties and hence exert an additional Earth system feedback (Schwinger et al. 2017).

i. UKESM1-0-LL

UKESM1-0-LL (Sellar et al. 2019) is the low resolution variant of the first version of the United Kingdom Earth System Model, a cutting edge full complexity ESM based on the HadGEM3-GC3 (Williams et al. 2018) physical global coupled model. The atmosphere component is vn11.2 of the Met Office Unified Model at 1.875 ° by 1.25 ° resolution with 85 levels in the vertical. The atmosphere includes the UK Chemistry and Aerosols (UKCA) model, configured for tropospheric (O'Connor et al. (2014)) and stratospheric (Morgenstern et al. (2017)) chemistry. Biogenic volatile organic compound (BVOCs) emissions from vegetation are included. The ocean model is NEMO vn3.6, at 1 ° resolution with 75 levels (Storkey et al. (2018)), with the CICE sea-ice model (Ridley et al. (2018)). The land component is vn5.2 of the JULES land surface model (Clark et al. (2011)), with terrestrial biogeochemistry represented by the dynamic vegetation model TRIFFID (Cox (2001),Wiltshire et al. (2020)) and the RothC four pool soil carbon model Coleman and Jenkinson (1999). TRIFFID and RothC represented the land carbon cycle in HadGEM2-ES (Collins et al. (2011)), the ESM used to perform the Met Office's contribution to CMIP5, but have undergone extensive development for inclusion in UKESM1. The number of natural plant functional types has risen to 9, and they now have a more realistic, plant trait based physiology (Harper et al. (2018)) employing new parameterizations based on observations of the TRY database (Kattge et al. (2011)).

The land carbon cycle is now coupled to the nitrogen cycle (Wiltshire et al. (2020). There are four soil organic carbon pools which decay at different rates, with four equivalent organic nitrogen pools, and an additional inorganic nitrogen pool. Mineralisation and immobilisation are simulated, allowing transfer of nitrogen between the organic and inorganic nitrogen pools. The inorganic nitrogen pool is available to PFTs to satisfy their nutrient demand; if insufficient inorganic soil nitrogen is available, net primary productivity is reduced, impacting plant biomass and leaf area index; the carbon which could not be assimilated due to nitrogen limitation is put into an exudates pool.

Land use in UKESM1 is represented by two crop and two pasture PFTs (Robertson (2020)). As the area of land devoted to agriculture grows, trees and shrubs are cleared away and put into three wood product pools with fast, medium, and slow decay rates. Crop PFTs are not nitrogen limited, assuming perfect application of nitrogenous fertilizer, and crop harvest is simulated by diverting 30 percent of crop litter from the soil. When run in emissions-driven configuration the harvest flux, exudates and decay from wood product pools are added to the atmosphere but are diagnostic only in CO_2 concentration-driven mode.

Ocean biogeochemistry is simulated by the MEDUSA-2 model (Yool et al. 2013). MEDUSA-2 includes two large and two small classes each of phytoplankton and zooplankton. Nutrients of nitrogen, silica, and iron are represented, in addition to dissolved inorganic carbon, oxygen, and alkalinity. Dust from the land surface provides an input of iron nutrient to the ocean.

SUPPLEMENTARY TABLES

Supplementary Table 1. **Change in global mean temperature** at 2100 relative to 1850-1899 mean for the 8 SSPs as simulated by the nine ESMs

Supplementary Table 2. **Net biosphere production** from the ESMs in the historical period compared with GCB2019 (Friedlingstein et al. (2019))

Supplementary Table 3. **Change in land carbon store** simulated by the ESMs for the historical period from 1850 to 2015 and for the SSPs from 1850 to 2100 compared with data form GCB2019 (Friedlingstein et al. (2019))

Supplementary Table 4. **Ocean carbon uptake** from the ESMs in the historical period compared with GCB2019 (Friedlingstein et al. (2019))

Supplementary Table 5. **Change in ocean carbon store** simulated by the ESMs for the historical period from 1850 to 2014 and for the SSPs from 1850 to 2100 compared with data from GCB2019 (Friedlingstein et al. (2019))

SUPPLEMENTARY TABLE 1. Change in global mean temperature (°C) at 2100 relative to 1850-1899 mean for the 8 SSPs as simulated by the nine ESMs, calculated from 11 year running means of ensemble means. Numbers in brackets indicate the maximum temperature reached if this differs from the 2100 value.

	ssp1-1.9	ssp1-2.6	ssp2-4.5	ssp3-7.0	ssp4-3.4	ssp4-6.0	ssp5-3.4over	ssp5-8.5
ACCESS-ESM1.5	-	2.0 (2.2)	3.1 (3.2)	4.5	-	-	-	5.2
CanESM5	2.2 (2.6)	2.8 (3.0)	4.4	6.6	3.8 (4.0)	5.4 (5.5)	3.5 (4.1)	7.9
CESM2	-	2.4	3.5	4.6	-	-	-	6.3
CNRM-ESM2-1	1.7	1.9 (2.2)	3.3	4.7	2.5 (2.6)	3.9	2.6 (2.8)	5.8
IPSL-CM6A-LR	1.8 (2.3)	2.4 (2.6)	3.8	5.5	3.0 (3.1)	4.3 (4.4)	2.8 (3.3)	6.8
MIROC-ES2L	1.5 (1.7)	1.5 (2.0)	2.6 (2.8)	3.5 (3.7)	-	-	-	4.7
MPI-ESM1.2-LR	-	1.4 (1.7)	2.5 (2.6)	3.7	-	-	-	4.4 (4.5)
NorESM2-LM	-	1.1 (1.5)	2.1	3.4	-	-	-	3.7 (4.0)
UKESM-0-LL	2.2 (2.4)	2.8	4.2	6.3	3.6 (3.7)	-	3.4 (3.7)	7.2
Mean	1.9	2.0	3.1	4.6	3.2	4.5	2.9	5.6

SUPPLEMENTARY TABLE 2. Net biosphere production (GtC yr^{-1}) averaged over the decades indicated. The equivalent flux from Table 6 of Friedlingstein et al. (2019), calculated as (S_{LAND}–E_{LUC}) is shown for the same periods, with the exception that the final value from Friedlingstein et al. (2019) covers 2009-2018 as opposed to 2009-2015 for the ESMs.

	1960s	1970s	1980s	1990s	2000s	2009-2015
GCB2019	-0.2±0.9	0.9±0.8	0.6±0.9	1.0±0.8	1.3±0.9	1.7±0.9
ACCESS-ESM1.5	0.98	0.92	1.24	1.25	1.11	1.07
CanESM5	-0.68	-0.36	-0.22	0.61	0.45	0.56
CESM2	-0.44	0.28	0.64	1.13	1.36	1.03
CNRM-ESM2-1	1.06	1.61	1.68	2.12	2.24	2.14
IPSL-CM6A-LR	-0.12	0.36	0.63	1.23	1.42	1.48
MIROC-ES2L	0.74	1.41	2.03	2.68	2.21	2.10
MPI-ESM1.2-LR	-0.33	-0.03	0.62	0.95	1.22	1.04
NorESM2-LM	-0.41	0.39	0.68	1.04	1.48	1.30
UKESM1-0-LL	-0.41	-0.08	0.26	0.76	0.93	1.00
Mean ± Std dev	0.04 ±0.68	0.5±0.68	0.84±0.70	1.318±0.67	1.38±0.57	1.30±0.53

SUPPLEMENTARY TABLE 3. Change in land carbon store (GtC) for the historical period from 1850 to 2015 and for the SSPs from 1850 to 2100. Data-based estimates from 1850 to 2014 are taken from Table 8 of Friedlingstein et al. (2019) as [S_{LAND} - E_{LUC}]

	Historical	ssp1-1.9	ssp1-2.6	ssp2-4.5	ssp3-7.0	ssp4-3.4	ssp4-6.0	ssp5-3.4over	ssp5-8.5
ACCESS-ESM1.5	98	-	152	142	88	-	-	-	124
CanESM5	-23	63	145	266	368	12	288	132	561
CESM2	-35	-	154	179	154	-	-	-	270
CNRM-ESM2-1	142	267	323	404	395	277	389	403	482
IPSL-CM6A-LR	25	138	186	201	170	84	177	134	196
MIROC-ES2L	33	92	155	254	368	-	-	-	406
MPI-ESM1.2-LR	-22	-	138	162	176	-	-	-	233
NorESM2-LM	-28	-	175	198	175	-	-	-	295
UKESM1-0-LL	-10	38	75	96	58	-27	-	57	107
Model mean	20±62	120±90	167±66	211±89	217±126	87±135	285±106	194±148	298±157
GCB2019	-10±60	-	-	-	-	-	-	-	-

SUPPLEMENTARY TABLE 4. Ocean carbon uptake (GtC yr^{-1}) averaged over the decades indicated. Ocean sink (S_{OCEAN}) from table 6 of Friedlingstein et al. (2019) is shown for the same periods, with the exception that the final value from the Friedlingstein et al. (2019) covers 2008-2017.

	1960s	1970s	1980s	1990s	2000s	2008-2015
GCB2018	1.0±0.5	1.3±0.5	1.7±0.5	2.0±0.5	2.1±0.5	2.4±0.5
ACCESS-ESM1.5	0.97	1.43	1.86	2.07	2.38	2.54
CanESM5	0.88	1.25	1.62	1.78	2.03	2.22
CESM2	0.89	1.28	1.68	1.84	2.12	2.35
CNRM-ESM2-1	0.75	1.17	1.49	1.71	2.02	2.21
IPSL-CM6A-LR	0.81	1.19	1.58	1.78	2.07	2.30
MIROC-ES2L	0.81	1.21	1.72	1.84	2.15	2.43
MPI-ESM1.2-LR	0.88	1.25	1.59	1.78	2.13	2.37
NorEMS2-LM	0.89	1.27	1.67	1.88	2.15	2.31
UKESM1-0-LL	0.93	1.26	1.70	1.82	2.10	2.35
Mean ± Std dev	0.86±0.06	1.235±0.04	1.63±0.08	1.80±0.05	2.10±0.05	2.32±0.07

SUPPLEMENTARY TABLE 5. Change in ocean carbon store (GtC) simulated by the nine ESMs for the historical period from 1850 to 2014 and for the SSPs from 1850 to 2100. Data-based estimates are from Friedlingstein et al. (2019), citing the IPCC estimate (Denman et al. 2007).

	Historical	ssp1-1.9	ssp1-2.6	ssp2-4.5	ssp3-7.0	ssp4-3.4	ssp4-6.0	ssp5-3.4over	ssp5-8.5
ACCESS-ESM1.5	150	-	319	419	514	-	-	-	583
CanESM5	132	231	278	366	448	292	389	329	506
CESM2	133	-	295	384	473	-	-	-	527
CNRM-ESM2-1	124	237	285	369	451	300	394	335	508
IPSL-CM6A-LR	128	244	293	384	470	311	410	350	534
MIROC-ES2L	131	257	302	394	478	-	-	-	531
MPI-ESM1.2-LR	134	-	301	388	471	-	-	-	534
NorESM2-LM	134	-	299	391	481	-	-	-	544
UKESM-0-LL	134	237	284	373	457	299	-	336	518
Mean ± Std dev	129±16	241±10	287±27	375±36	458±47	301±8	397±11	337±9	516±53
GCB2019	150±20	-	-	-	-	-	-	-	-

SUPPLEMENTARY FIGURES

Supplementary Figure 1. Change in **historical global mean surface air temperature**.

Supplementary Figure 2. Change in **global mean temperature** under the SSPs.

Supplementary Figure 3. **Fossil fuel CO_2 emissions rate** compatible with the SSPs.

Supplementary Figure 4. **Cumulative fossil fuel CO_2 emissions** compatible with the SSPs.

Supplementary Figure 5. Timeseries of **Net Biosphere Productivity** under the SSPs.

Supplementary Figure 6. Change in **land carbon store** under the SSPs.

Supplementary Figure 7. Change in **soil carbon store** under the SSPs.

Supplementary Figure 8. Change in **vegetation carbon store** under the SSPs.

Supplementary Figure 9. Change in **litter carbon store** under the SSPs.

Supplementary Figure 10. Timeseries of **air-to-sea flux of CO_2** under the SSPs.

Supplementary Figure 11. Change in **ocean carbon store** under the SSPs.

Supplementary Figure 12. **Cumulative Airborne Fraction** of fossil fuel CO_2 emissions under the SSPs.

Supplementary Figure 13. Historical **FF emissions and Cumulative FF emissions**

Supplementary Figure 14. Historical **LUC emissions and cumulative LUC emissions** from paired expts

Supplementary Figure 15. Historical **FF + LUC emissions and cumulative FF + LUC emissions**

Supplementary Figure 1. Change in global mean surface air temperature (°C) relative to 1850-1899 mean for the historical period as simulated by the 9 ESMs.

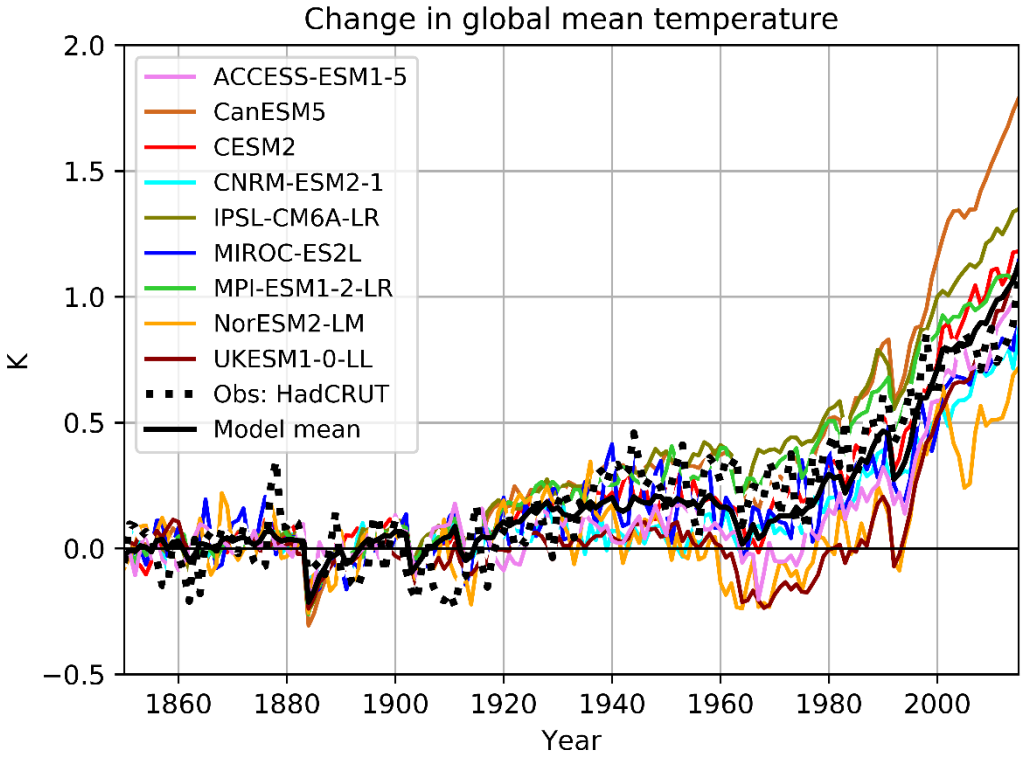

Supplementary Figure 2. Change in global mean temperature for the 9 ESMs individually for all SSP experiments performed by each relative to the 1850-1899 mean of the *historical* ensemble mean of each model. Dashed horizontal lines indicate 1.5 ˚C and 2.0 ˚C of warming

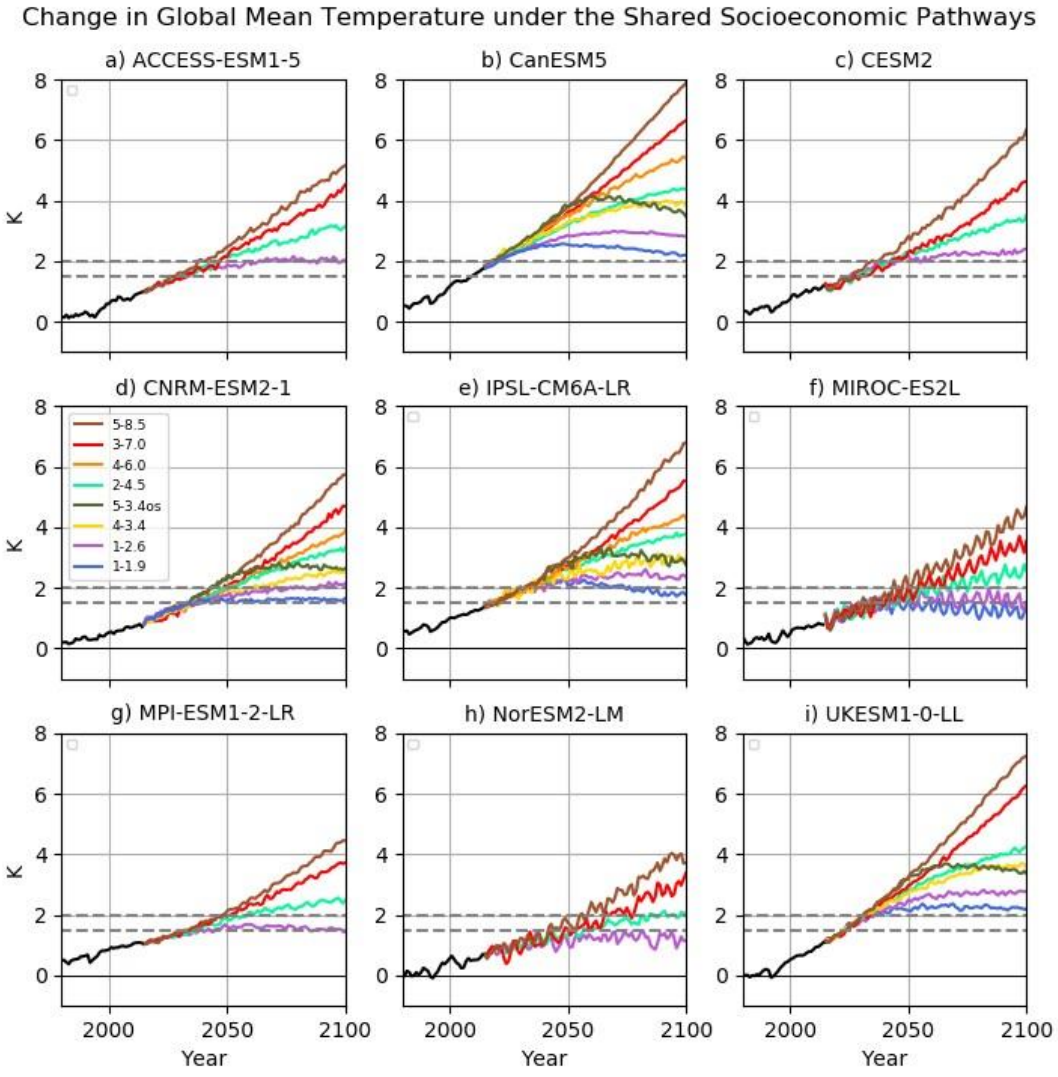

Supplementary Figure 3. Fossil fuel CO_2 emissions rate compatible with the Shared Socioeconomic Pathways.

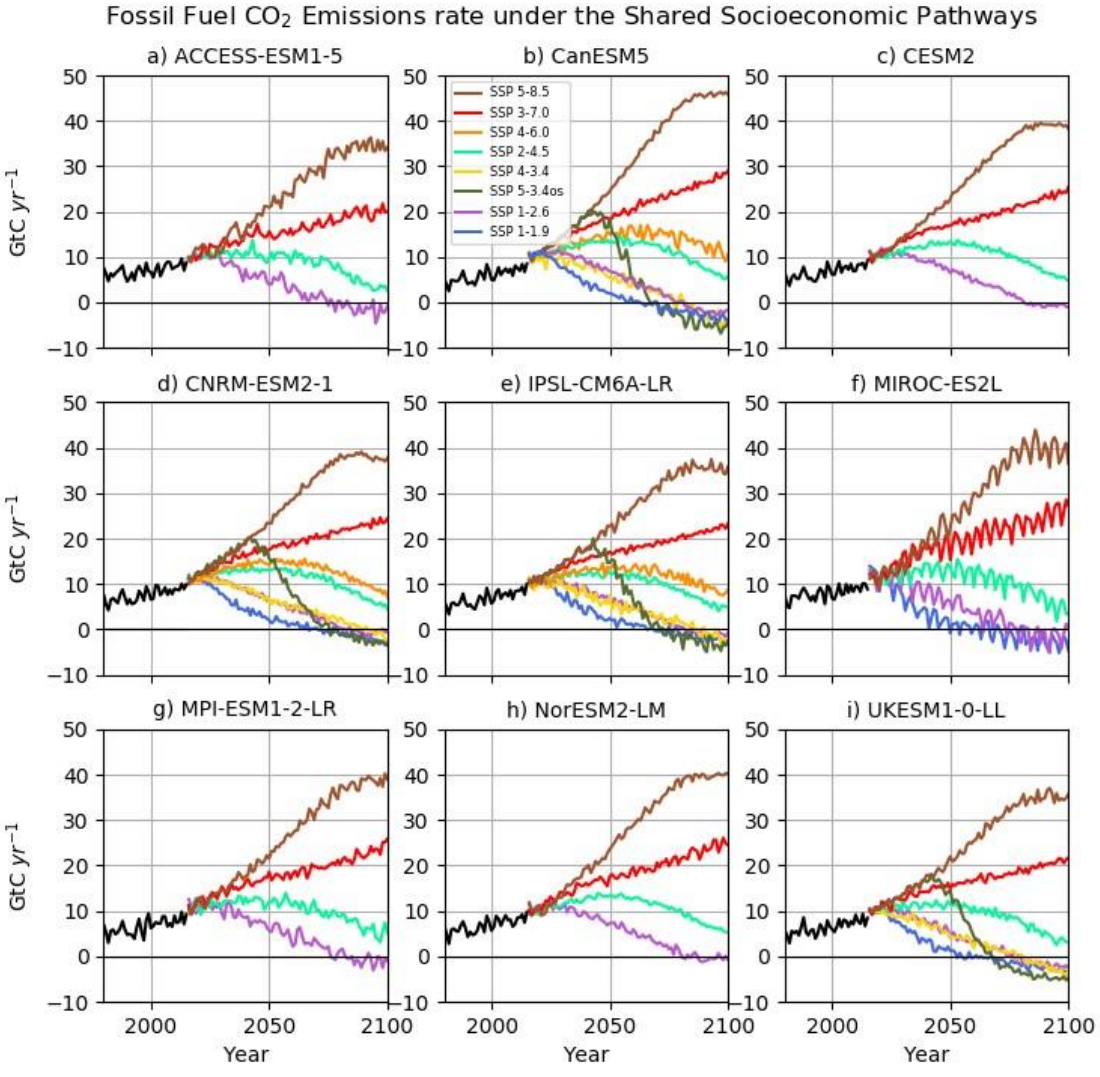

Supplementary Figure 4. Cumulative fossil fuel CO_2 emissions compatible with the Shared Socioeconomic Pathways

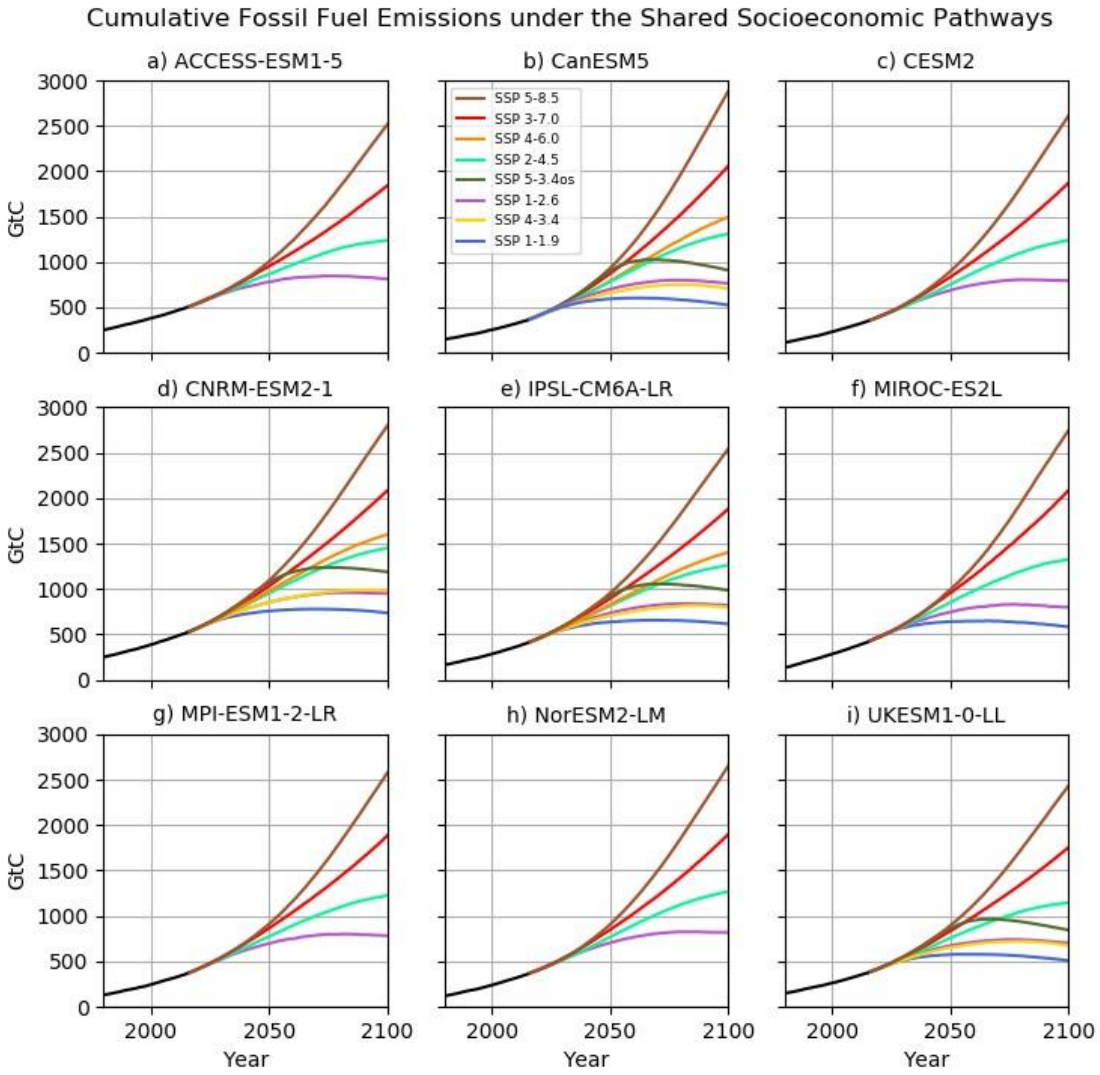

Supplementary Figure 5. Timeseries of Net Biosphere Productivity under the Shared Socioeconomic Pathways.

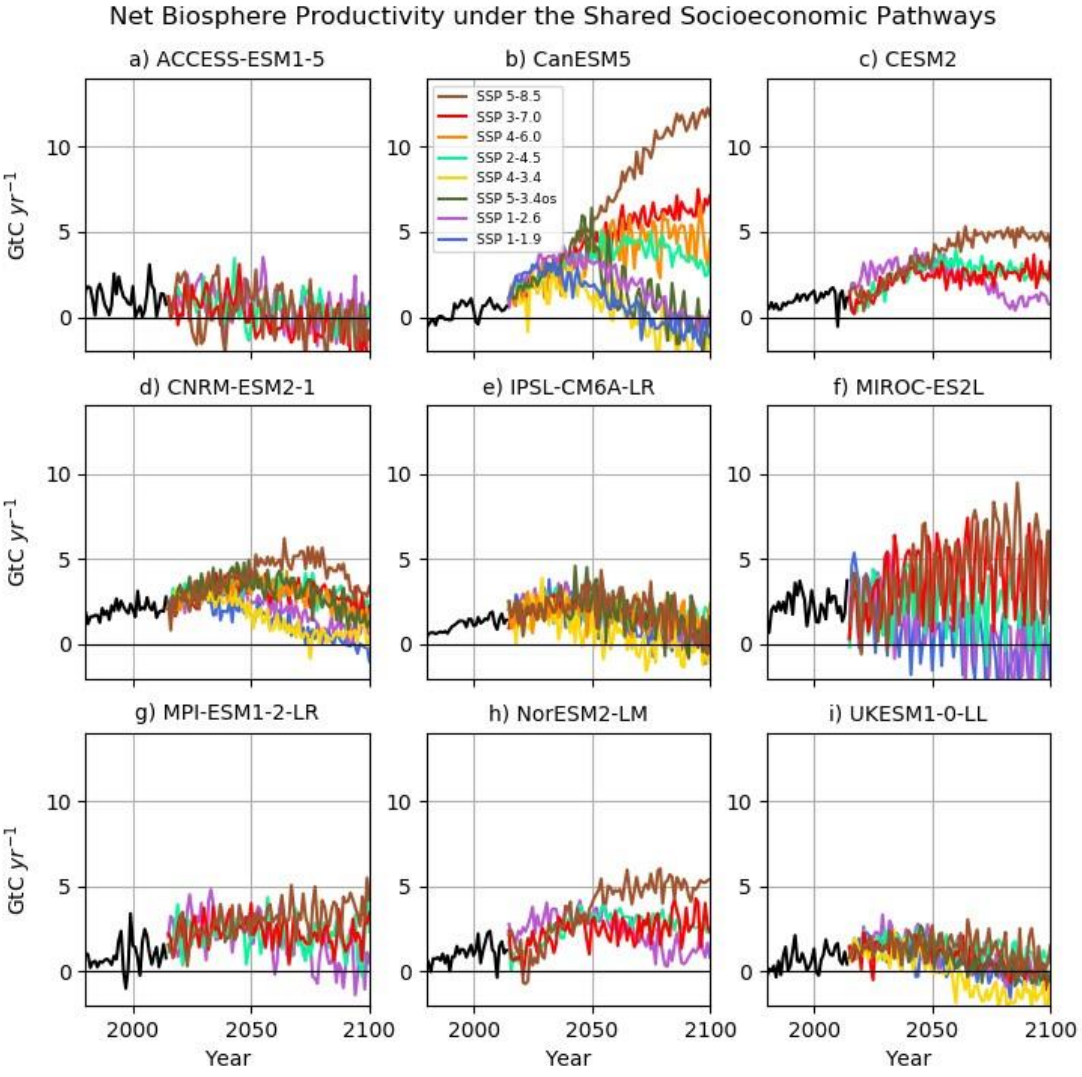

Supplementary Figure 6. Change in land carbon store under the Shared Socioeconomic Pathways.

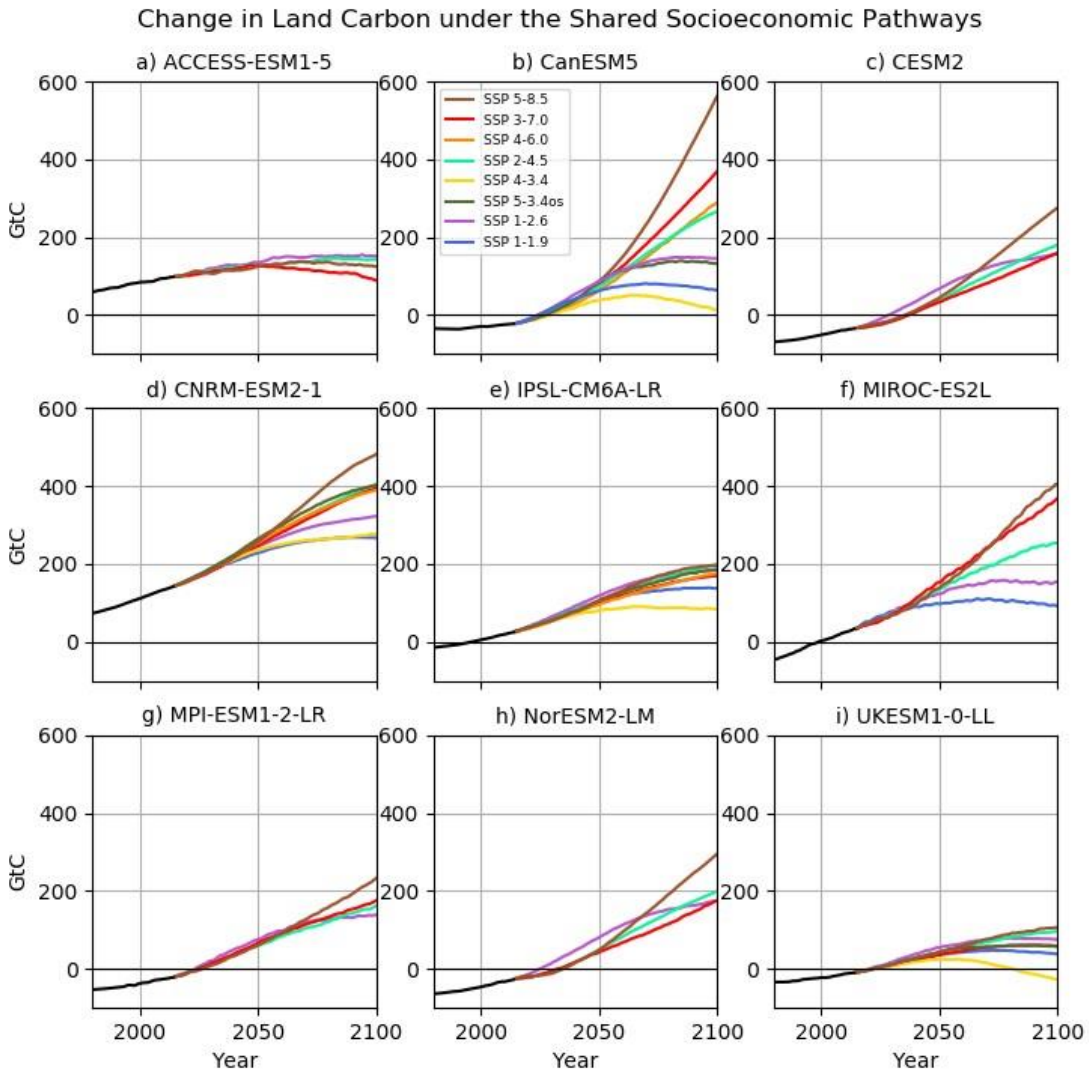

Supplementary Figure 7. Change in soil carbon store under the Shared Socioeconomic Pathways.

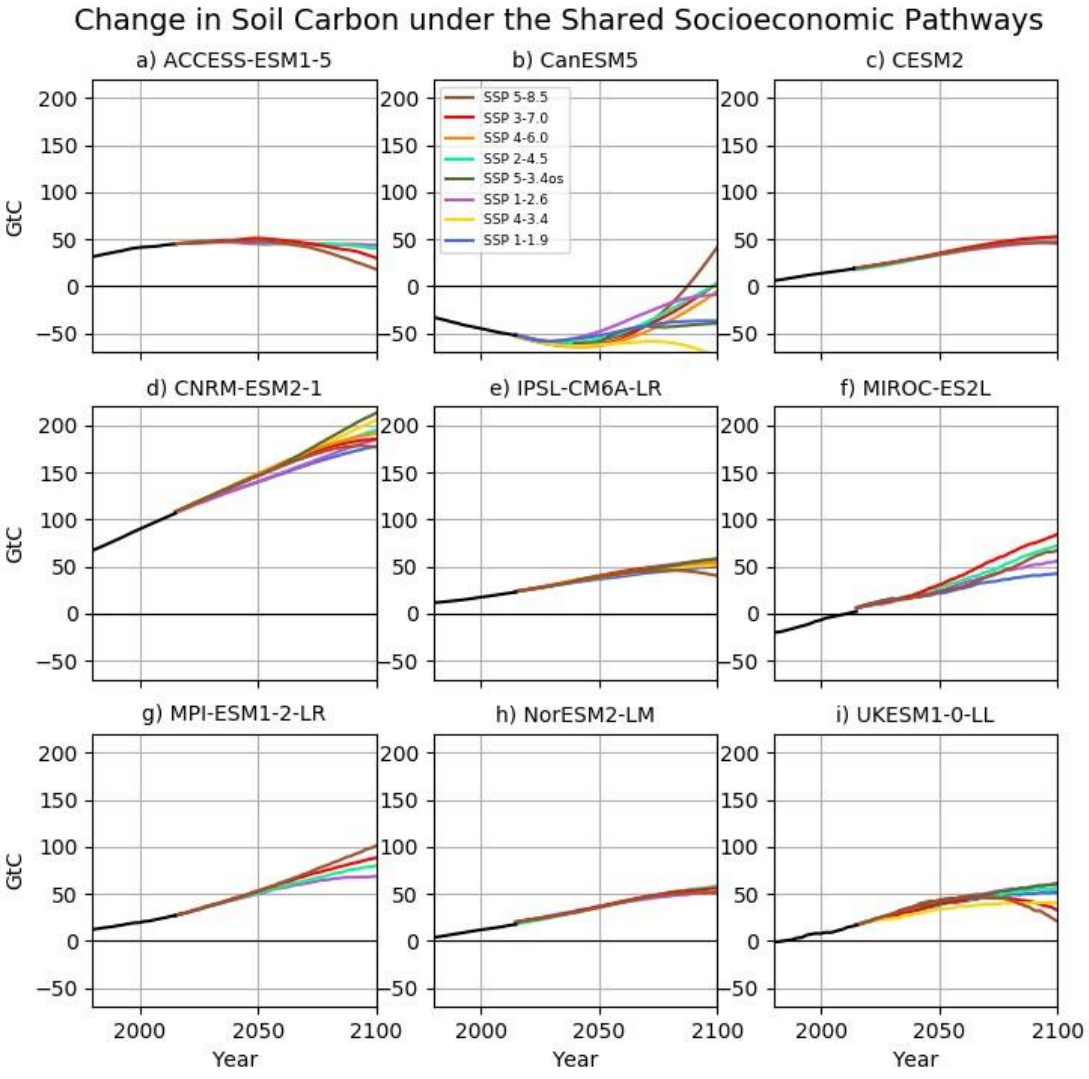

Supplementary Figure 8. Change in vegetation carbon store under the Shared Socioeconomic Pathways.

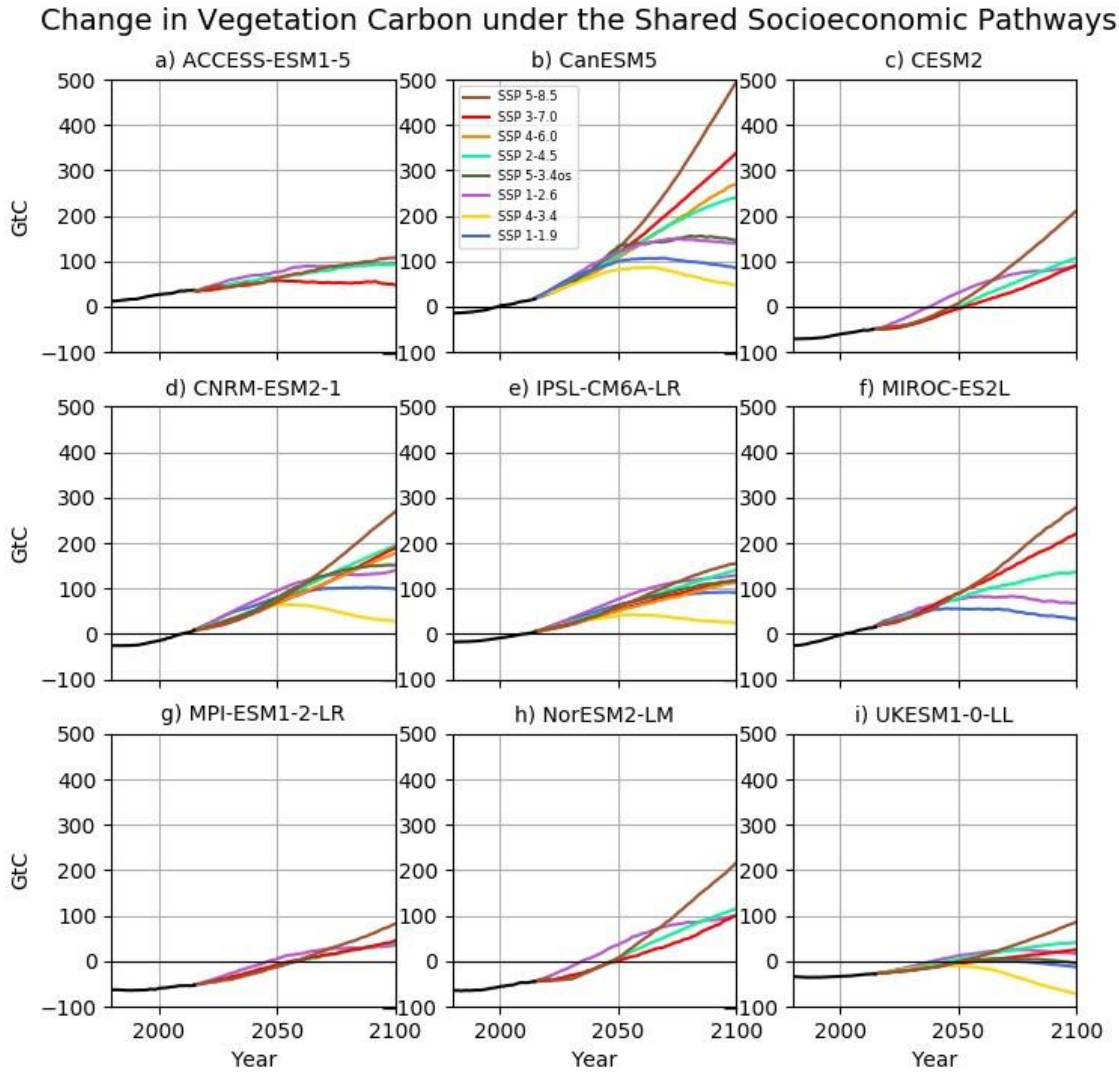

Supplementary Figure 9. Change in litter carbon store under the Shared Socioeconomic Pathways.

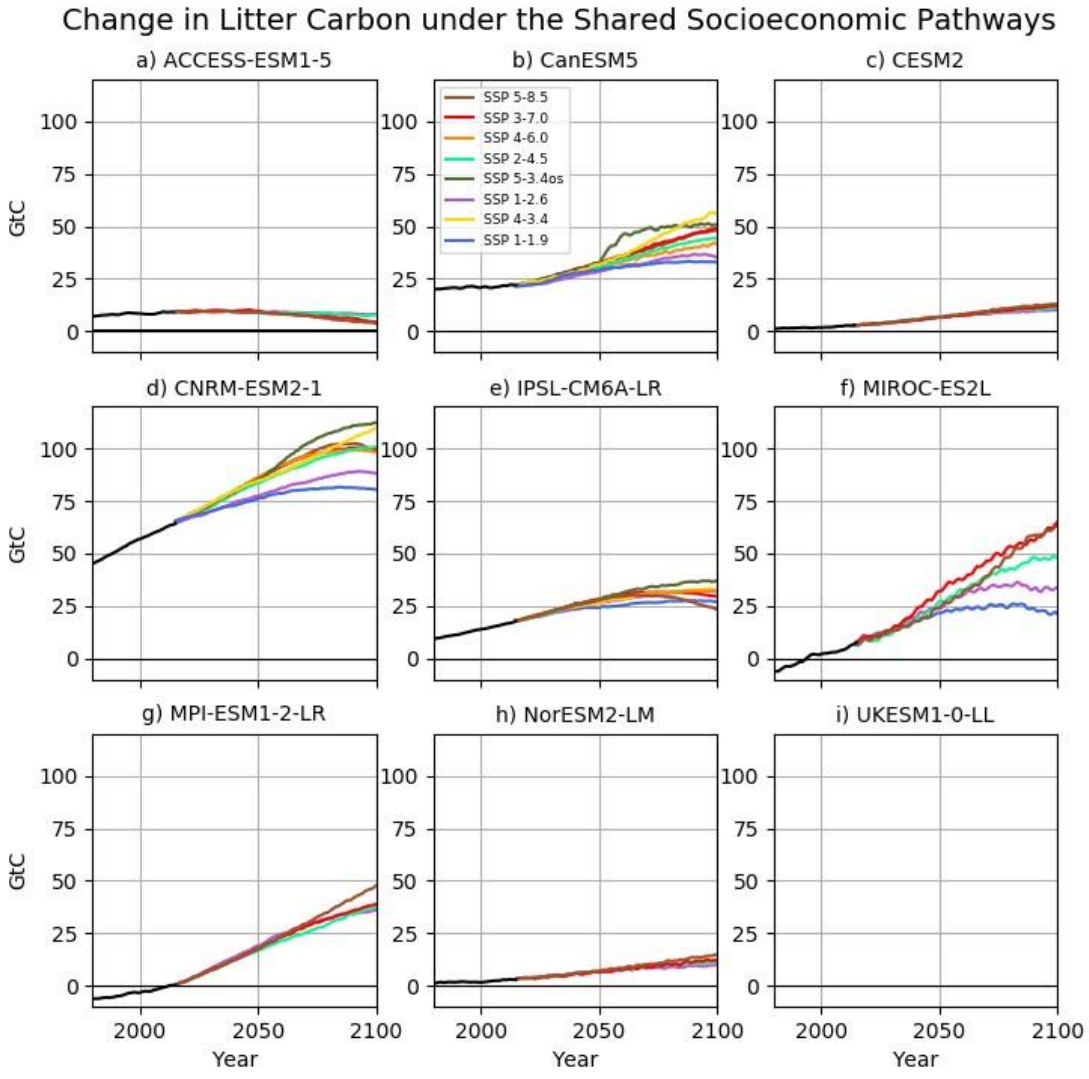

Supplementary Figure 10. Timeseries of air-to-sea flux of CO_2 under the Shared Socioeconomic Pathways.

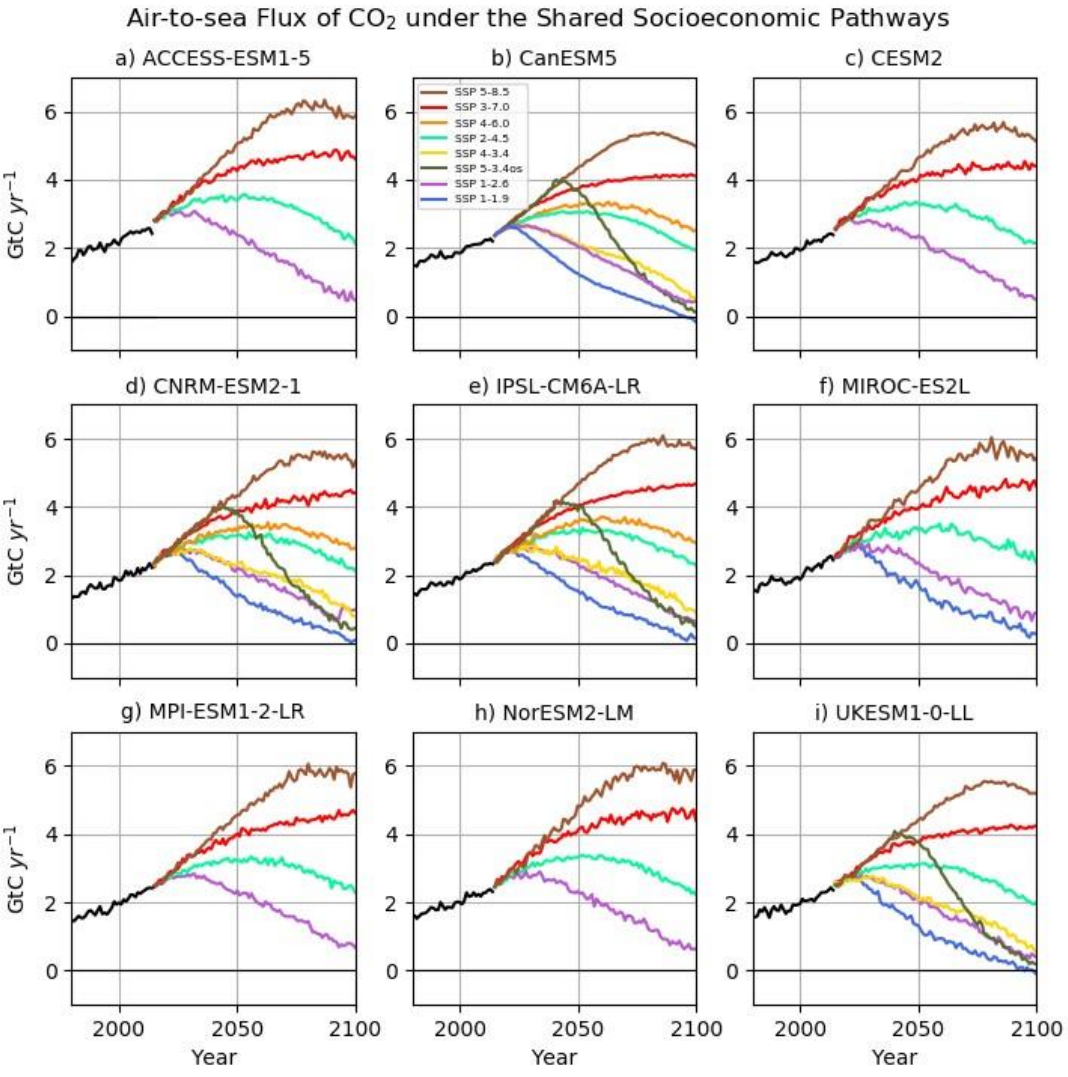

Supplementary Figure 11. Change in ocean carbon store under the Shared Socioeconomic Pathways.

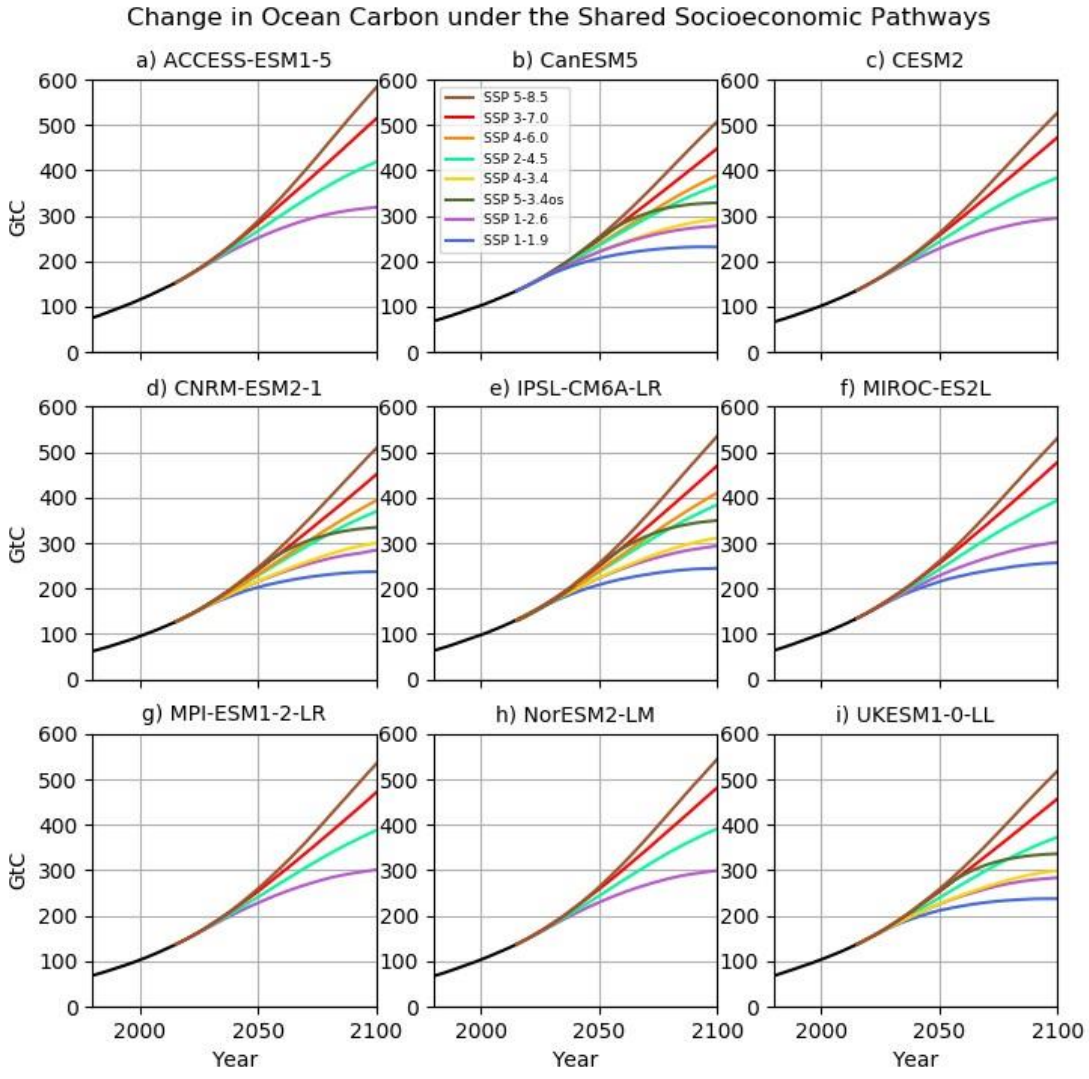

Supplementary Figure 12. Cumulative Airborne Fraction of fossil fuel CO_2 emissions under the Shared Socioeconomic Pathways.

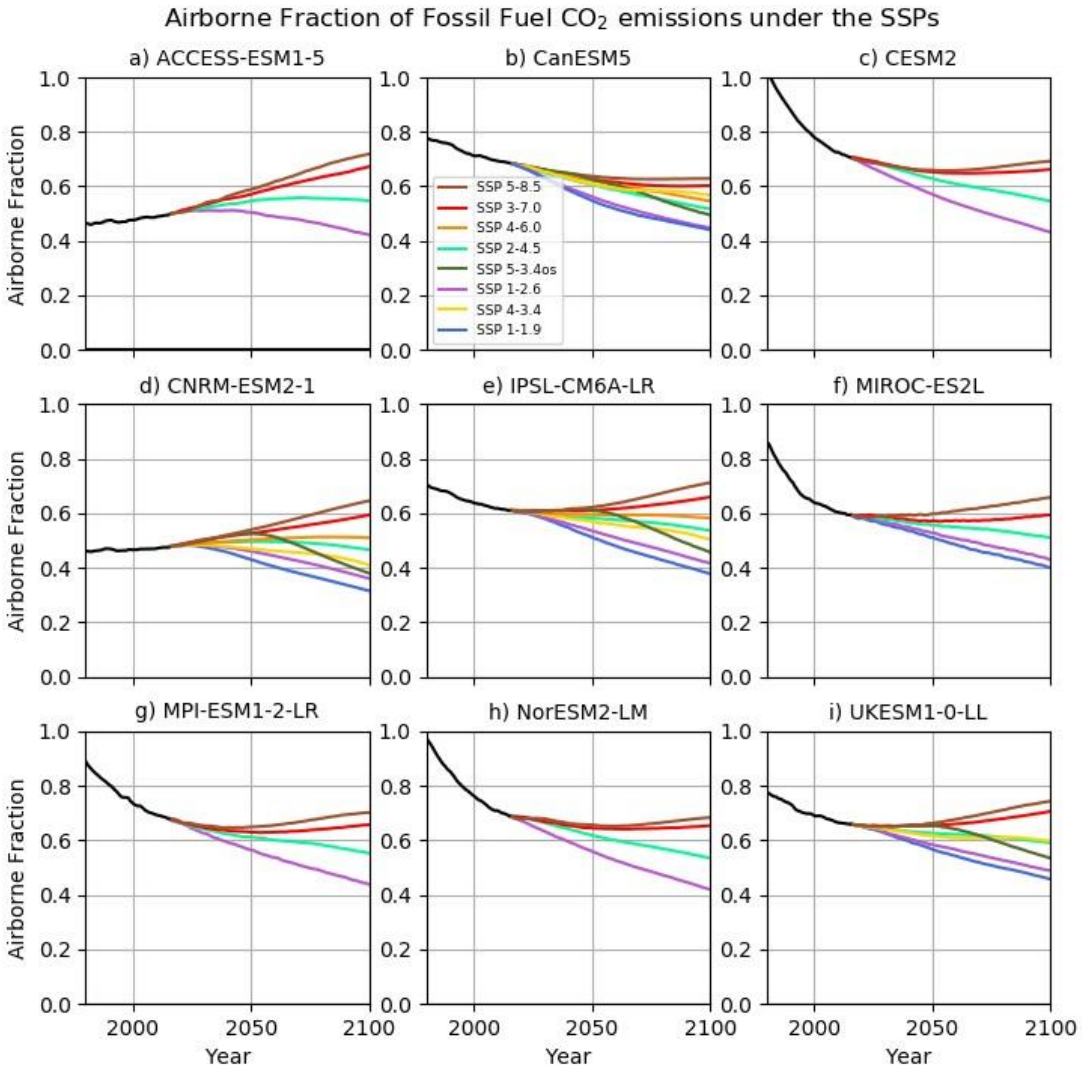

Supplementary Figure 13. Enlarged version of Figure 3 (a) and (b) from the main text. Timeseries (left panel) and cumulative total (right panel) of fossil fuel CO_2 emissions from CanESM5, CESM2, CNRM, IPSL, and UKESM with observational fossil fuel emissions from Gilfillan et al (2019).

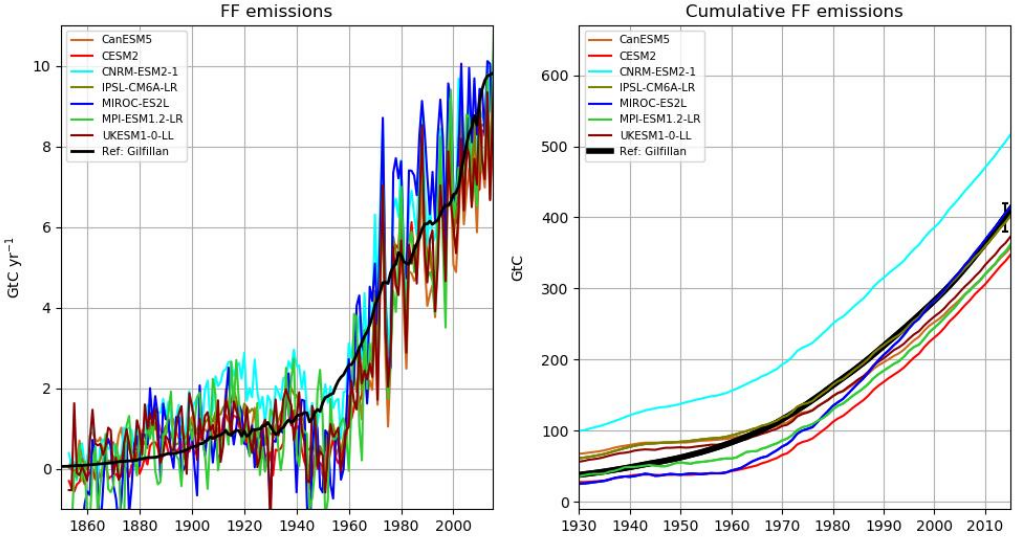

Supplementary Figure 14. Enlarged version of Figure 3 (c) and (d) from the main text. Timeseries (left panel) and cumulative total (right panel) of land use emissions calculated as land carbon uptake (cumulative NBP) in *hist-noLu* minus that in *historical.* The black curve is the dataset of land use emissions provided under the C4MIP protocols for driving the emissions-driven historical *esm-hist* experiment for models which do not have the ability to simulate LUC emissions interactively with the atmosphere. These are derived from Hansis et al. (2015) and Houghton et al (2012). The green curve is land use emissions from GCB2019 (Friedlingstein et al (2019)), the cumulative total calculated using Table 8.

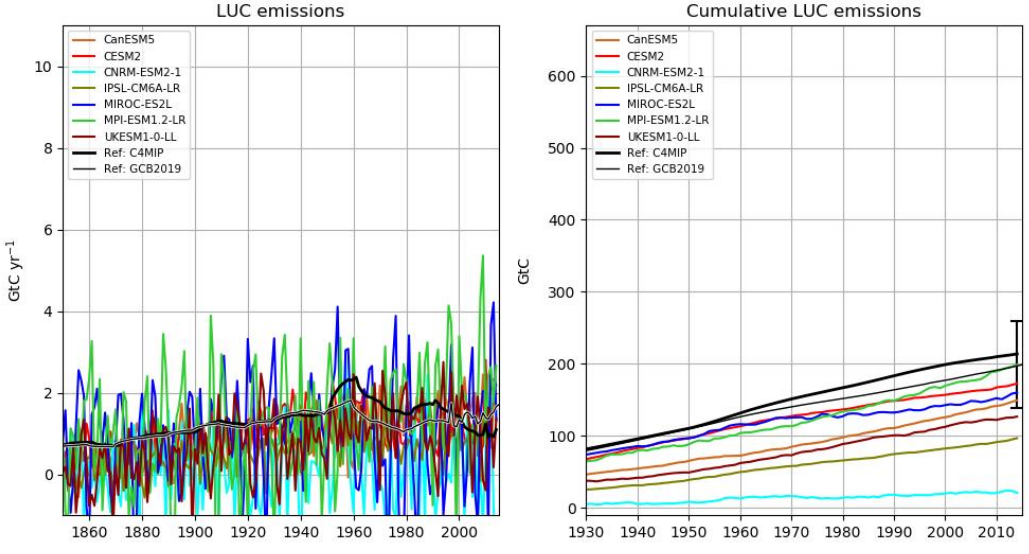

Supplementary Figure 15. Enlarged version of Figure 3 (e) and (f) from the main text. Timeseries (left panel) and cumulative total (right panel) of the sum of fossil fuel emissions + land use emissions shown in Supplementary Figures 13 and 14.

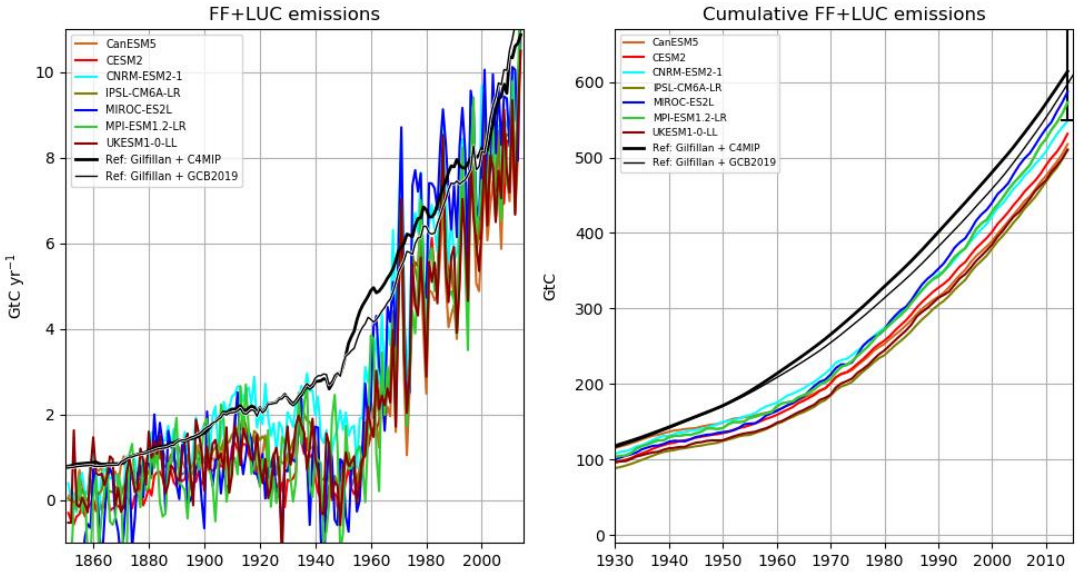

References

Arora, V. K., and G. J. Boer, 2005: Fire as an interactive component of dynamic vegetation models. *Journal of Geophysical Research: Biogeosciences*, 110 (G2), doi:10.1029/2005JG000042, URL https://agupubs.onlinelibrary.wiley.com/doi/abs/10.1029/2005JG000042.

Arora, V. K., and G. J. Boer, 2010: Uncertainties in the 20th century carbon budget associated with land use change. *Global Change Biology*, 16 (12), 3327–3348, URL https://onlinelibrary.wiley.com/doi/abs/10.1111/j.1365-2486.2010.02202.x.

Arora, V. K., J. R. Melton, and D. Plummer, 2018: An assessment of natural methane fluxes simulated by the CLASS-CTEM model. *Biogeosciences*, 15 (15), 4683–4709, URL https://www.biogeosciences.net/15/4683/2018/ .

Arora, V. K., and J. F. Scinocca, 2016: Constraining the strength of the terrestrial co_2 fertilization effect in the Canadian earth system model version 4.2 (CanESM4.2). *Geoscientific Model Development*, 9 (7), 2357–2376, URL https://www.geosci-model-dev.net/9/2357/2016/.

Arora, V. K., and Coauthors, 2011: Carbon emission limits required to satisfy future representative concentration pathways of greenhouse gases. *Geophysical Research Letters*, 38 (5), https://agupubs.onlinelibrary.wiley.com/doi/pdf/10.1029/2010GL046270 .

Aumont, O., C. Ethe, A. Tagliabue, L. Bopp, and M. Gehlen, 2015: PISCES-v2: an ocean biogeochemical model for carbon and ecosystem studies. 8, 2465–2513, doi:10.5194/gmd-8-2465-2015.

Bouillon, S., M. A. Morales Maqueda, V. Legat, and T. Fichefet, 2009: An elastic-viscous-plastic sea ice model formulated on Arakawa B and C grids. *Ocean Modelling*, 27 (3), 174–184, doi: 10.1016/j.ocemod.2009.01.004.

Christian, J. R., and Coauthors, 2010: The global carbon cycle in the canadian earth system model *(canesm1): Preindustrial control simulation.* Journal of Geophysical Research: Biogeosciences,115 (G3), https://agupubs.onlinelibrary.wiley.com/doi/abs/10.1029/2008JG000920

Clark, D. B., and Coauthors, 2011: The Joint UK Land Environment Simulator (JULES), model description – part 2: Carbon fluxes and vegetation dynamics. *Geoscientific Model Development*, 4 (3), 701–722, doi:10.5194/gmd-4-701-2011, URL https://www.geosci-model-dev.net/4/701/2011/

Coleman, K., and D. S. Jenkinson, 1999: RothC-26.3 - a model for the turnover of carbon in soil: Model description and users guide, Rothamsted Research, Harpenden, U.K. URL https://www.rothamsted.ac.uk/sites/default/files/RothC guide WIN.pdf .

Collatz, G. J., M. Ribas-Carbo, and J. A. Berry, 1992: Coupled photosynthesis-stomatal conductance model for leaves of C4 plants. *Aust. J. Plant Physiol.*, 19, 519–539, doi:10.1071/PP9920519.

Collins, W., and Coauthors, 2011: Development and evaluation of an earth system model, hadgem2. *Geoscientific Model Development*, 4, 1051–1075, doi:10.5194/gmd-4-1051-2011.

Cox, P., 2001: Description of the triffid dynamic global vegetation model, Hadley Centre Technical Note 24, UK Met Office. https://www.researchgate.net/publication/245877262_Description_of_the_TRIFFID_dynamic_global_vegetation_model .

Cramer, W., 1997: Using plant functional types in a global vegetation model*, 271–288. Cambridge* University Press.

Danabasoglu, G., J. Lamarque, J. Bacmeister, D. A. Bailey, A. DuVivier, J. Edwards, and co authors, 2020: The community earth system model version 2 (CESM2). *J. Adv. Model. Earth Syst.*, 12, doi:doi:10.1029/2019MS001916.

Decharme, B., and Coauthors, 2019: Recent changes in the ISBA-CTRIP land surface system for use in the CNRM-CM6 climate model and in global off-line hydrological applications. *Journal of Advances in Modeling Earth Systems*, 11 (5), 1207–1252, doi:10.1029/2018MS001545, URL https://agupubs.onlinelibrary.wiley.com/doi/abs/10.1029/2018MS001545 .

Delire, C., R. Séférian, B. Decharme, R. Alkama, D. Carrer, E. Joetzjer, X. Morel, and M. Rocher, 2019: The global land carbon cycle simulated with isba. *Journal of Advances in Modeling Earth Systems*.

Denman, K., and Coauthors, 2007: *Couplings Between Changes in the Climate System and Biogeochemistry*, Vol. 2007, 499–587.

Farquhar, G. D., S. Von Caemmerer, and J. A. Berry, 1980: A biochemical model of photosynthetic CO_2 assimilation in leaves of C3 species. *Planta*, 149, 78–90.

Fichefet, T., and M. A. M. Maqueda, 1997: Sensitivity of a global sea ice model to the treatment *of ice thermodynamics and dynamics.* Journal of Geophysical Research: Oceans*, 102 (C6),* 12609–12646, https://agupubs.onlinelibrary.wiley.com/doi/abs/10.1029/97JC00480 .

Friedlingstein, P., and Coauthors, 2019: Global carbon budget 2019. *Earth System Science Data*, 11 (4), 1783–1838, doi:10.5194/essd-11-1783-2019, https://www.earth-syst-sci-data.net/11/1783/2019/ .

Goll, D. S., V. Brovkin, J. Liski, T. Raddatz, T. Thum, and K. E. O. Todd-Brown, 2015: Strong dependence of CO2 emissions from anthropogenic land cover change on initial land cover and soil carbon parametrization. *Global Biogeochemical Cycles*, 29 (9), 1511–1523, https://agupubs.onlinelibrary.wiley.com/doi/pdf/10.1002/2014GB004988 .

Goll, D. S., A. J. Winkler, T. Raddatz, N. Dong, I. C. Prentice, P. Ciais, and V. Brovkin, 2017: Carbon–nitrogen interactions in idealized simulations with JSBACH (version 3.10). *Geoscientific Model Development*, 10 (5), 2009–2030, doi:10.5194/gmd-10-2009-2017, URL https://gmd.copernicus.org/articles/10/2009/2017/ .

Goudriaan, J., H. van Laar, H. van Keulen, and W. Louwerse, 1985: *Photosynthesis, C02 and plant production.*, A, Vol. 86, 107–122. In W. Day R.K. Atkin (Eds.), Wheat growth and modelling. NATO AS Series, Series A.

Hagemann, S., and T. Stacke, 2015: Impact of the soil hydrology scheme on simulated soil moisture memory. *Climate Dynamics*, 44, 1731–1750, doi:doi:10.1007/s00382-014-2221-6.

Harper, A. B., and Coauthors, 2018: Vegetation distribution and terrestrial carbon cycle in a carbon cycle configuration of jules4.6 with new plant functional types. *Geoscientific Model Development*, 11 (7), 2857–2873, doi:10.5194/gmd-11-2857-2018, https://www.geosci-model-dev.net/11/2857/2018/ .

Houghton, R. A., J. I. House, J. Pongratz, G. R. van der Werf, R. S. DeFries, M. C. Hansen,914C. Le Quéré, and N. Ramankutty, 2012: Carbon emissions from land use and land-cover change. 91541 Biogeosciences,9 (12), 5125–5142, doi:10.5194/bg-9-5125-2012, https://bg.copernicus.916org/articles/9/5125/2012/

Hurtt, G. C., and Coauthors, 2020: Harmonization of global land-use change and management for the period 850–2100 (LUH2) for cmip6. *Geoscientific Model Development Discussions*, 2020, 1–65, doi:10.5194/gmd-2019-360, URL https://gmd.copernicus.org/preprints/gmd-2019-360/ .

Ilyina, T., K. D. Six, J. Segschneider, E. Maier-Reimer, H. Li, and I. Nunez-Riboni, 2013: Global ocean biogeochemistry model HAMOCC: Model architecture and performance as component of the MPI-earth system model in different CMIP5 experimental realizations. *Journal of Advances in Modeling Earth Systems*, 5 (2), 287–315, doi:10.1029/2012MS000178, https://agupubs.onlinelibrary.wiley.com/doi/abs/10.1029/2012MS000178

Kattge, J., S. D´ıaz, and e. a. Lavorel, S, 2011: Try – a global database of plant traits. *Glob Change Biol.*, 17(9), 2905–2935, doi:doi:10.1111/j.1365-2486.2011.02451.x.

Kirkevag, A., and Coauthors, 2018: A production-tagged aerosol module for earth system models, OsloAero5.3 – extensions and updates for CAM5.3-Oslo. *Geoscientific Model Development*, 11 (10), 3945–3982, doi:10.5194/gmd-11-3945-2018, https://gmd.copernicus.org/articles/11/3945/2018/

Krinner, G., and Coauthors, 2005: A dynamic global vegetation model for studies of the coupled atmosphere-biosphere system. *gbc*, 19 (1), GB1015, doi:10.1029/2003GB002199.

Lasslop, G., K. Thonicke, and S. Kloster, 2014: Spitfire within the MPI earth system model: Model development and evaluation. *Journal of Advances in Modeling Earth Systems*, 6 (3), 740–755, doi:10.1002/2013MS000284, https://agupubs.onlinelibrary.wiley.com/doi/pdf/10.1002/2013MS000284 .

Lawrence, D. M., and Coauthors, 2019: The community land model version 5: Description of new features, benchmarking, and impact of forcing uncertainty. *Journal of Advances in Modeling Earth Systems*, 11 (12), 4245–4287, doi:10.1029/2018MS001583, https://agupubs.https://agupubs.onlinelibrary.wiley.com/doi/pdf/10.1029/2018MS001583.

Madec, G., R. Bourdalle-Badie, P. Bouttier, C. Bricaud, D. Bruciaferri, D. Calvert, and M. Vancoppenolle, 2017: NEMO ocean engine (version v3.6). *Notes du Pole de modelisation de l'Institut´ Pierre-simon Laplace (IPSL)*, doi:10.5281/zenodo.1472492.

Maier-Reimer, E., Kriest, I., Segschneider, J. and Wetzel, P.: The Hamburg ocean carbon cycle model HamOCC5.1 - technical description, Max Planck Institute for Meteorology, Hamburg, Germany. Tech. rep.

Mauritsen, T., and Coauthors, 2019: Developments in the mpi-m earth system model version 1.2 (mpi-esm1.2) and its response to increasing CO2. *Journal of Advances in Modeling Earth Systems*, 11 (4), 998–1038, doi:10.1029/2018MS001400, URL https://agupubs.onlinelibrary.wiley.com/doi/abs/10.1029/2018MS001400 .

Morgenstern, O., and Coauthors, 2017: Review of the global models used within phase 1 of the chemistry–climate model initiative (ccmi). *Geosci. Model Dev.*, 10(2), 639--671, doi:10.5194/gmd-10-639-2017.

O'Connor, F. M., and Coauthors, 2014: Evaluation of the new ukca climate-composition model – Part 2: The troposphere. *Geosci. Model Dev.*, 7(1), 41–91, doi:10.5194/gmd-7-41-2014.

Parton, W. J., J. W. B. Stewart, and C. V. Cole, 1988: Dynamics of c, n, p and s in grassland soils: a model. *Biogeochemistry*, 5 (1), 109–131, doi:10.1007/BF02180320, https://doi.org/10.1007/BF02180320 .

Paulsen, H., Ilyina, T., Six, K. D., and Stemmler, I. (2017), Incorporating a prognostic representation of marine nitrogen fixers into the global ocean biogeochemical model HAMOCC, J. Adv. Model. Earth Syst., 9, 438– 464, doi:10.1002/2016MS000737.

Peylin, P., and Coauthors, 2020: The ORCHIDEE global land surface model version v2.0: description and evaluation. *in prep for GMD*.

Prentice, I., W. Cramer, S. Harrison, R. Leemans, R. Monserud, and A. Solomon, 1992: A global biome model based on plant physiology and dominance: Soil properties and climate. *J. Biogeogr.*, 19, 117–134, doi:10.2307/2845499.

Reick, C. H., T. Raddatz, V. Brovkin, and V. Gayler (2013), Representation of natural and anthropogenic land cover change in MPI-ESM, J. Adv. Model. Earth Syst., 5, 459–482, doi:10.1002/jame.20022

Ridley, J. K., E. W. Blockley, A. B. Keen, J. G. L. Rae, A. E. West, and D. Schroeder, 2018: The sea ice model component of hadgem3-gc3.1. *Geosci. Model Dev.*, 11(2), 713–723, doi:10.5194/gmd-11-713-2018.

Robertson, E., Wiltshire, A. J. and Liddicoat, S. K., 2021: A New Representation of Land use in the JULES Land Surface Model. *Geosci. Model Dev.*
Rousset, C., and Coauthors, 2015: The Louvain-La-Neuve sea ice model LIM3.6: global and regional capabilities. 28, 2991–3005, doi:10.5194/gmd-8-2991-2015.

Salas-Melia, D., 2002: A global coupled sea ice-ocean model. *Ocean Modelling*, 4, 137–172.
Schwinger, J., J. Tjiputra, N. Goris, K. D. Six, A. Kirkevag, Ø. Seland, C. Heinze, and T. Ilyina,2017: Amplification of global warming through ph dependence of dms production simulated with a fully coupled earth system model. *Biogeosciences*, 14 (15), 3633–3648, doi:10.5194/bg-14-3633-2017, URL https://bg.copernicus.org/articles/14/3633/2017/ .

Seland, Ø., and Coauthors, 2020: The norwegian earth system model, noresm2 – evaluation of the cmip6 deck and historical simulations. *Geoscientific Model Development Discussions*, 2020, 1–68, doi:10.5194/gmd-2019-378, https://gmd.copernicus.org/preprints/gmd-2019-378/.

Sellar, A. A., Jones, C. G., Mulcahy, J. P., Tang, Y., Yool, A., Wiltshire, A., et al. (2019). UKESM1: Description and evaluation of the U.K. Earth System Model. Journal of Advances in Modeling Earth Systems, 11, 4513– 4558. https://doi.org/10.1029/2019MS001739

Sellers, P. J., and Coauthors, 1996: Comparison of radiative and physiological effects of doubled atmospheric CO_2 on climate. *Science*, 271, 1402–1406, doi:10.1126/science.271.5254.1402.
Storkey, D., and Coauthors, 2018: Uk global ocean go6 and go7: a traceable hierarchy of model resolutions. *Geosci. Model Dev.*, 11(8), 3187—-3213, doi:10.5194/gmd-11-3187-2018.

Swart, N. C., and Coauthors, 2019: The canadian earth system model version 5 (canesm5.0.3). *Geoscientific Model Development*, 12 (11), 4823–4873, doi:10.5194/gmd-12-4823-2019, URL https://www.geosci-model-dev.net/12/4823/2019/.

Séférian, R., and Coauthors, 2019: Evaluation of CNRM earth system model, CNRM-ESM2-1: Role of earth system processes in present-day and future climate. *Journal of Advances in Modeling*

Earth Systems, doi:10.1029/2019MS001791, URL https://agupubs.onlinelibrary.wiley.com/doi/abs/10.1029/2019MS001791 .

Tjiputra, J. F., and Coauthors, 2020: Ocean biogeochemistry in the Norwegian earth system model version 2 (NorESM2). *Geoscientific Model Development*, 13 (5), 2393–2431, doi: 10.5194/gmd-13-2393-2020, URL https://gmd.copernicus.org/articles/13/2393/2020/ .

Toniazzo, T., M. Bentsen, C. Craig, B. E. Eaton, J. Edwards, S. Goldhaber, C. Jablonowski, and P. H. Lauritzen, 2020: Enforcing conservation of axial angular momentum in the atmospheric general circulation model cam6. *Geoscientific Model Development*, 13 (2), 685–705, doi:10.5194/gmd-13-685-2020, URL https://gmd.copernicus.org/articles/13/685/2020/ .

Vancoppenolle, M., T. Fichefet, H. Goosse, S. Bouillon, G. Madec, and M. A. Morales Maqueda, 2009: Simulating the mass balance and salinity of Arctic and Antarctic sea ice. 1. Model description and validation. 27, 54–69, doi:10.1016/j.ocemod.2008.11.003.

Verseghy, D. L., 2000: The Canadian land surface scheme (class): Its history and future. A*tmosphere-Ocean*, 38 (1), 1–13, doi:10.1080/07055900.2000.9649637, URL https://doi.org/10.1080/07055900.2000.9649637 .

von Salzen, K., and Coauthors, 2013: The Canadian fourth generation atmospheric global climate model (canam4). part i: Representation of physical processes. *Atmosphere-Ocean*, 51 (1), 104–125, doi:10.1080/07055900.2012.755610, URL https://doi.org/10.1080/07055900.2012.755610).

Wanninkhof, R., 2014: Relationship between wind speed and gas exchange over the ocean revisited. *Limnology and Oceanography: Methods*, 12 (6), 351–362, doi:10.4319/lom.2014.12.351, https://aslopubs.onlinelibrary.wiley.com/doi/abs/10.4319/lom.2014.12.351 .

Williams, K. D., and Coauthors, 2018: The met office global coupled model 3.0 and 3.1 (gc3.0 and gc3.1) configurations. *J. Adv. Model. Earth Syst*, 10(2), 357–380, doi:10.1002/2017MS001115.

Wiltshire, A., and Coauthors, 2020: Jules-CN: a coupled terrestrial carbon-nitrogen scheme (jules vn5.1). doi:10.5194/gmd-2020-205 .

Wullschleger, S. D., and Coauthors, 2014: Plant functional types in earth system models: past experiences and future directions for application of dynamic vegetation models in high-latitude ecosystems. *Ann. Bot.-London*, 114, 1–16, doi:10.1093/aob/mcu077.

Yool, A., E. E. Popova, and T. R. Anderson, 2013: Medusa-2.0: an intermediate complexity biogeochemical model ofthe marine carbon cycle for climate change and ocean acidification studies. *Geosci. Model Dev.*, 6(5), 1767–1811, doi:10.5194/gmd-6-1767-2013.

Ziehn, T., and Coauthors, 2020: The australian earth system model: Access-esm1.5. *Journal of Southern Hemisphere Earth Systems Science (J. South. Hemisphere Earth Syst. Sci.)*, https://doi.org/10.1071/ES19035 .